GSA DATA REPOSITORY 2013274

Sea level induced seismicity and submarine landslide occurrence

Daniel S. Brothers[1], Karen M. Luttrell[2], Jason D. Chaytor[1]

1. US Geological Survey
   Coastal and Marine Science Center
   384 Woods Hole Rd
   Woods Hole, MA 02543
2. US Geological Survey
   Earthquake Science Center
   345 Middlefield Rd, MS 910
   Menlo Park, CA 94025

Stress Modeling Parameters

A full description of the underlying theory, methods and modeling assumptions used in the present paper are described in Luttrell and Sandwell (2010). For the Amazon margin, the structural cross-section and elastic plate thickness (*H*=35 km; Figure 3a) assigned to the models were based on results from Watts et al. (2009). As a conceptual illustration, Supplementary Figures S2 and S3 show how sensitive the ΔC_f models are to changes in elastic thickness (*H*=15, 35 and 50 km). The computation is semi-analytic in that it convolves the spatially-accurate shape of the ocean load due to 120 m of sea level rise with with a vertical Green's function describing the response of the subsurface to a point load (Smith and Sandwell, 2006; Luttrell and Sandwell, 2010). The effective elastic thickness (T_e) of a region determined by flexural modeling of gravity anomalies is a good proxy for lithosphere thickness (e.g., Watts 2001) and we therefore choose elastic plate thickness values (*H*) appropriate for each region based on studies estimating effective elastic thickness. The choice of *H* affects the flexural rigidity and flexural wavelength of the plate. Consequently, a thicker plate will affect a larger area around the coastline, whereas stresses in a thinner plate will be more localized. The models assume a Young's modulus of 70 GPa, a Poisson's ratio of 0.25, a mantle material density of 3300 $kg \cdot m^{-3}$ (Luttrell and Sandwell, 2010).

For simplicity all faults in our models are assigned a dip of 60°, the average dip for crystaline normal faults that comprise the dominant structural elements along these margins. Structural constraints on the Amazon and US Mid-Atlantic margins suggest that a 60° dip for thin-skinned faults is reasonable (Klitgord and Hutchinson, 1988; Watts et al., 2009). The effect of wide variations in dip angle (e.g., 30º - 80º) is second order relative to the effects of elastic plate thickness, fault location relative to the coastline, and dip direction (e.g., toward or away from the ocean load). The coefficient of friction for crystalline and thin-skinned faults in the model are set to μ=0.6 and μ=0.1, respectively; thin-skinned faults are expected to be weak and less capable of generating large earthquakes.

Tables and Figures

Table DR1. Catalog of published age constraints for major submarine landslides along glacial and non-glacial margins, and the approximate cessation age of coarse-grained deposition on deep-sea fan systems. See below for expanded reference list.

Figure DR1. Structural cross-sections for (**a**) the Amazon margin (based on Watts et al., 2009) and (**b**) the North Carolina margin (based on Hutchinson and Klitgord, 1988) that were used in stress models (Figures 3 and 4a; Supp. Figures S2 and S3). Coulomb failure stress (ΔC_f) models across the Amazon margin (**b-d**) based on Watts et al. (2009). See Supp. Text for a detailed description of model parameters. The basement hinge-zone defines the landward edge of the marginal sedimentary basins. Structures within the hinge-zone include half-grabens with seaward dipping border faults, tilted blocs and syn-rift sedimentary wedges that formed primarily during Mesozoic rifting. Seaward of the hinge zone, growth faults are observed in the post-rift sedimentary section and appear to accommodate gravitational collapse of the sedimentary wedge and differential subsidence across the margin (Klitgord and Hutchinson, 1988; Steckler et al., 1988). Transitional crust separates the continental crust (30—40 km) from thinner oceanic crust (5–10 km thick).

Figure DR2. Coulomb failure stress (ΔC_f) models across the Amazon margin. Elastic thickness (H) is varied across panels **a**, **b** and **c** to show the show the sensitivity in ΔC_f across various fault systems. Regardless of the elastic thickness used, fault rupture is promoted along at least one fault system within 100 km of the shelf-edge. Numbered stars are receiver faults whose ΔC_f time variations are shown in Supp. Figure S3. See Supp. Text for a detailed description of model parameters.

Figure DR3. (a) Eustatic sea level curve of Peltier and Fairbanks (2006). (b–d) Load induced ΔC_f for six different receiver faults (see corresponding numbers in Supp. Figure S2) using H=15, 35 and 50 km.

Supplementary Table DR1: Submarine Mass Transport Age Constraints

Large-scale glacial landslides

Map #	*Name*	*Age (kyr BP)*	*Reference*
8	Grand Banks	0.07	Piper et al. (1999)
12	Logan Canyon 1	0.84 ± 0.05	Jenner et al. (2007)
1	Traenadjupet	4.1 ± 0.1	Laberg et al. (2002)
13	Logan Canyon 2	5.7 ± 0.1	Jenner et al. (2007)
4	Afen	5.8 ± 0.1	Wilson et al. (2004)
3	Storegga	8.1 ± 0.3	Haflidason et al. (2005)
5	Faeroe	9.9 ± 0.1	Van Weering et al. (1998)
11	Verrill Canyon	~10	Piper et al (2003)
6	Peach	16.8 ± 2.1	Holmes et al. (1998)
10	Verrill Canyon	~12	Piper et al (2003)
9	Verrill Canyon	14 to 15	Piper et al (2003)
2	Nyk	16.3 ± 0.1	Lindberg et al. (2004)
7	Rockall	15 to 16	Flood et al. (1979)
14	South Whale basin	22 to 24	Piper et al. (2003)
N/A	Hinlopen	~30	Winkleman (2007)

Large-scale non-glacial landslides

Map #	*Name*	*Age (kyr BP)*	*Reference*
10	Nice Airport	0.03	Dan et al. (2007)
1	Baltimore-Norfolk Canyon	5.3 ± 0.15	Embley (1982)
1	Baltimore-Norfolk Canyon	6.7 ± 0.3	Embley (1982)
1	Baltimore-Norfolk Canyon	7.3 ± 0.3	Embley (1982)
1	Baltimore-Norfolk Canyon	10 ± 0.5	Embley (1982)
12	BIG '95	11.3 ± 0.3	Canals et al. (2004), Lastras et al. (2004)
3	Cape Fear	8 to 14	Embley (1980); Popenoe et al. (1993); Paull et al. (1996); Rodriguez and Paull (2000)
9	Canary	15 ± 2	Masson (2006)
8	Saharan	15 to 16	Embley (1982)
4	Amazon Shallow E	14 to 17	Maslin et al. (1998)
5	Amazon Shallow W	14 to 17	Maslin et al. (1998)
2	Currituck	25 to 50	Prior et al. (1986)
6	Amazon Deep E	~35	Maslin et al. (1998)
7	Amazon Deep W	42 to 45	Maslin et al. (1998)
8	Saharan	~60	Gee et al. (1999)
11	Ana	~61.5	Berndt et al. (2012)

Deep-sea fan mass transport deposits

Map #	*Name*	*Age (kyr BP)*	*Reference*
7	Nile	9 to 10	Garziglia et al. (2008)
4	Mauritania	10.5 to 10.9	Henrich et al. (2008)
9	Celtic	7 to 12	Zaragosi et al. (2000)
2	Mississippi	11 to 12	Kolla and Perlmutter (1993); Schwab et al. (1996); Twichell et al. (1992)
3	Amazon	13.3 ± 0.6	Flood (1991)
6	Tyrrhenian	~13.8	Trincardi et al (2003)
5	Madiera	~15	Weaver et al. (1983)
1	Black Shell (Hatteras)	15.9 ± 0.3	Elmore et al. (1979)
8	Horseshoe Abysal Plain	~17.7	Lebreiro et al. (1997)

Figure DR1

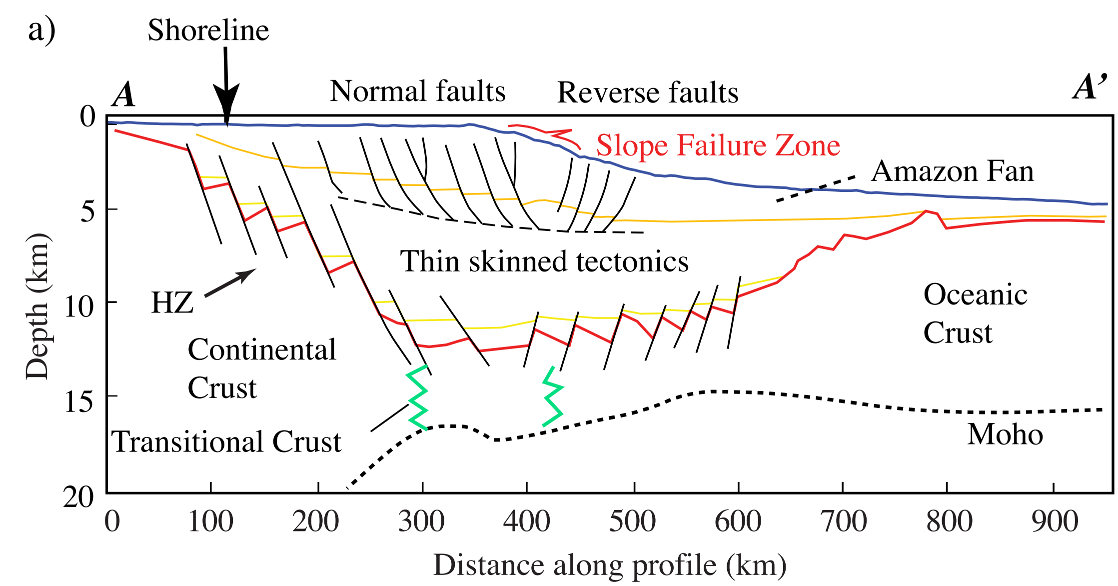

a)
Shoreline
A
A’
Normal faults
Reverse faults
Slope Failure Zone
Amazon Fan
Thin skinned tectonics
HZ
Continental
Crust
Oceanic
Crust
Transitional Crust
Moho
Depth (km)
0
5
10
15
20
0
100
200
300
400
500
600
700
800
900
Distance along profile (km)

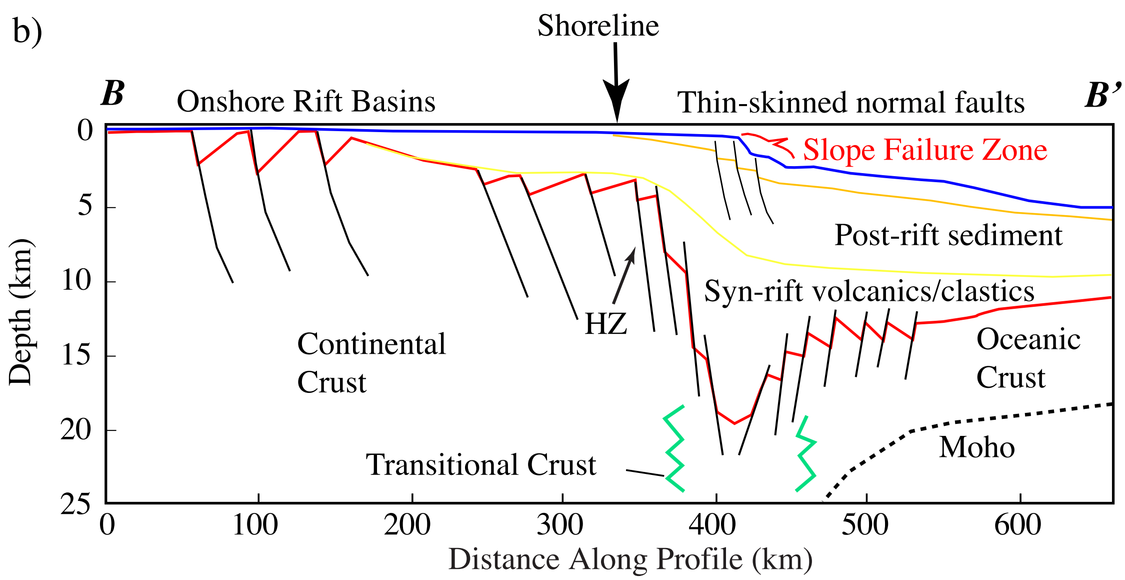

b)
Shoreline
B
B’
Onshore Rift Basins
Thin-skinned normal faults
Slope Failure Zone
Post-rift sediment
Syn-rift volcanics/clastics
HZ
Continental
Crust
Oceanic
Crust
Transitional Crust
Moho
Depth (km)
0
5
10
15
20
25
0
100
200
300
400
500
600
Distance Along Profile (km)

Figure DR2

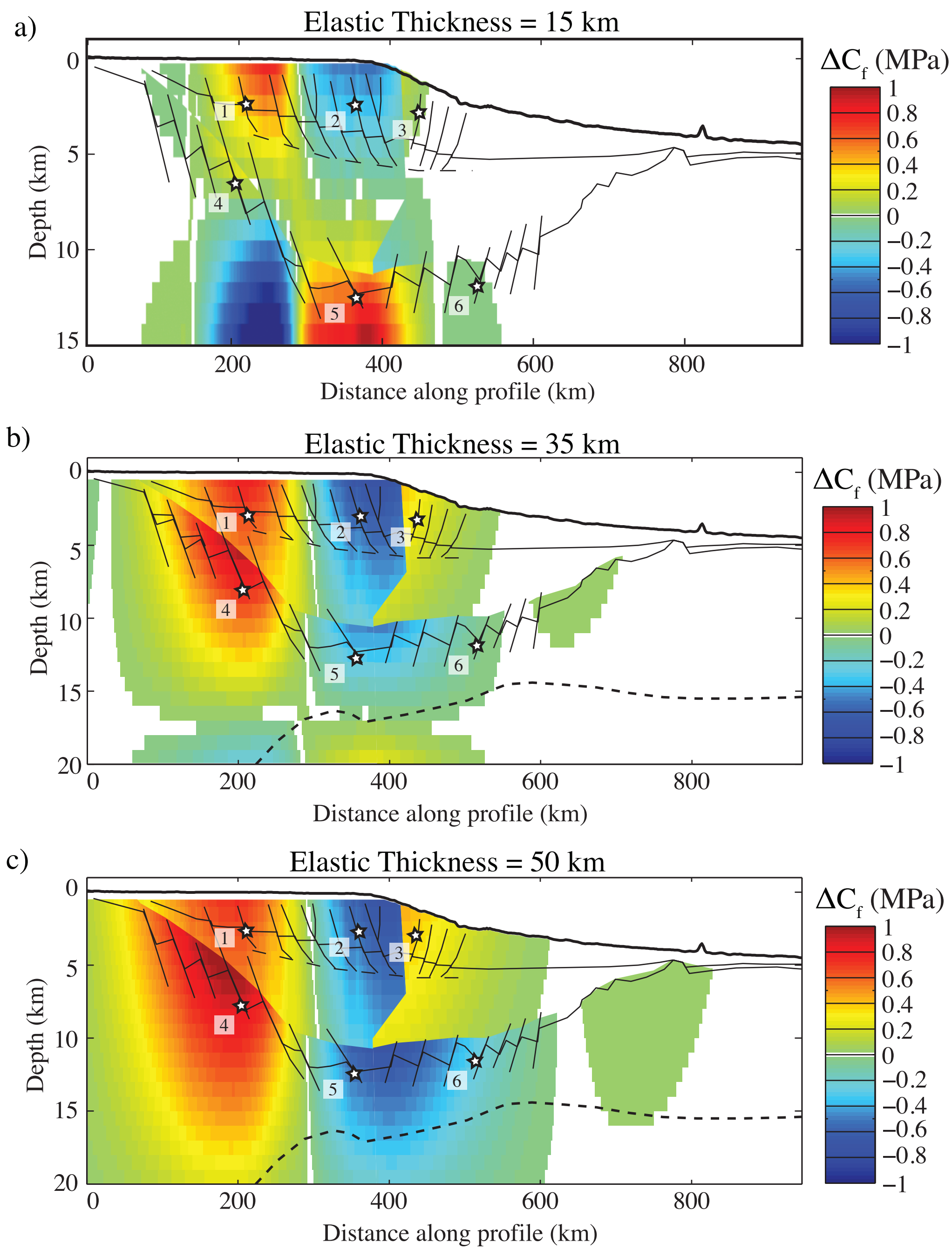
a)
Elastic Thickness = 15 km
b)
Elastic Thickness = 35 km
c)
Elastic Thickness = 50 km
Depth (km)
Distance along profile (km)
ΔC_f (MPa)
0
5
10
15
20
200
400
600
800
1
0.8
0.6
0.4
0.2
−0.2
−0.4
−0.6
−0.8
−1
1
2
3
4
5
6

Figure DR3

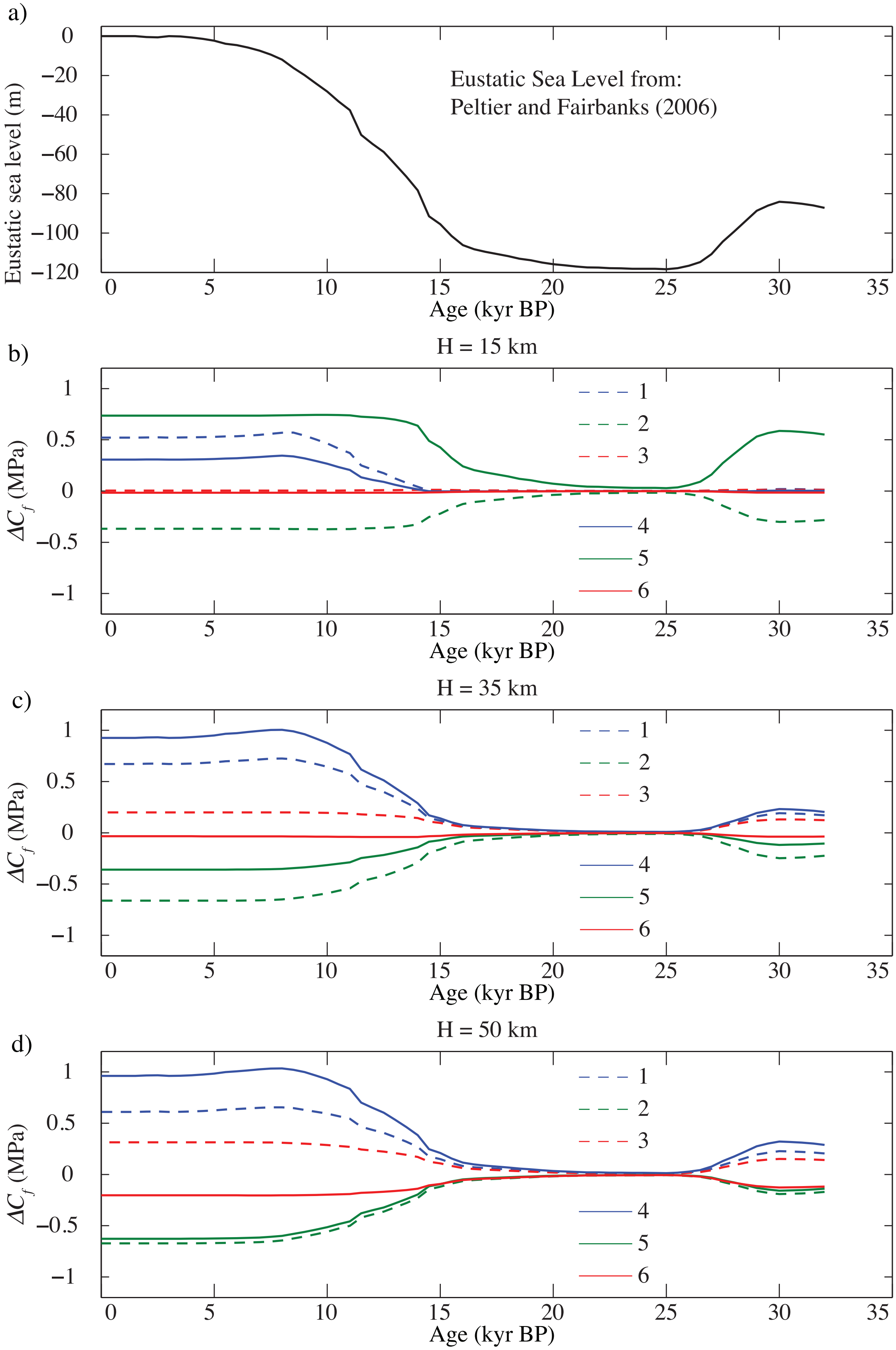

a)
Eustatic sea level (m)
0
−20
−40
−60
−80
−100
−120
0
5
10
15
20
25
30
35
Age (kyr BP)
Eustatic Sea Level from:
Peltier and Fairbanks (2006)
b)
H = 15 km
c)
H = 35 km
d)
H = 50 km
ΔCf (MPa)
1
0.5
0
−0.5
−1
1
2
3
4
5
6

Expanded Reference List

Supplementary Text, sites shown in Figure 2, and age data in Table DR1

Berndt, C., Costa, S., Canals, M., Camerlenghi, A., de Mol, B., Saunders, M., 2012. Repeated slope failure linked to fluid migration: The Ana submarine landslide complex, Eivissa Channel, Western Mediterranean Sea. Earth and Planetary Science Letters 319, 65-74.

Dan, G., Sultan, N., Savoye, B., 2007. The 1979 Nice harbour catastrophe revisited: Trigger mechanism inferred from geotechnical measurements and numerical modelling. Marine Geology 245, 40-64.

Elmore, R.D., Pilkey, O.H., Cleary, W.J., Curran, H.A., 1979. Black Shell turbidite, Hatteras Abyssal Plain, western Atlantic Ocean. Geological Society of America Bulletin 90, 1165-1176.

Embley, R.W., 1980. The Role of Mass-Transport in the Distribution and Character of Deep-Ocean Sediments with Special Reference to the North-Atlantic. Marine Geology 38, 23-50.

Flood, R.D., Manley, P.L., Kowsmann, R.O., Appi, C.J., Pirmez, C., 1991. Seismic facies and late Quaternary growth of Amazon submarine fan. Springer-Verlag, New York.

Garziglia, S., Migeon, S., Ducassou, E., Loncke, L., Mascle, J., 2008. Mass-transport deposits on the Rosetta province (NW Nile deep-sea turbidite system, Egyptian margin): Characteristics, distribution, and potential causal processes. Marine Geology 250, 180-198.

Gee, M.J.R., Masson, D.G., Watts, A.B., Allen, P.A., 1999. The Saharan debris flow: an insight into the mechanics of long runout submarine debris flows. Sedimentology 46, 317-335.

Grow, J.A., Sheridan, R.E., 1988. U.S. Atlantic continental margin; a typical Atlantic-type or passive contiental margin. Geological Society of America, Boulder.

Haflidason, H., Lien, R., Sejrup, H.P., Forsberg, C.F., Bryn, P., 2005. The dating and morphometry of the Storegga Slide. Marine and Petroleum Geology 22, 123-136.

Henrich, R., Hanebuth, T.J.J., Krastel, S., Neubert, N., Wynn, R.B., 2008. Architecture and sediment dynamics of the Mauritania Slide Complex. Marine and Petroleum Geology 25, 17-33.

Holmes, R., Long, D., Dodd, L.R., 1998. Large-scale debrites and submarine landslides on the Barra Fan, west of Britain. Geological Society, London, Special Publications 129, 67-79.

Jenner, K.A., Piper, D.J.W., Campbell, D.C., Mosher, D.C., 2007. Lithofacies and origin of late Quaternary mass transport deposits in submarine canyons, central Scotian Slope, Canada. Sedimentology 54, 19-38.

Klitgord, K.D., Hutchinson, D.R., 1988. U.S. Atlantic continental margin; structural and tectonic framework. Geological Society of America, Boulder.
Kolla, V., Perlmutter, M.A., 1993. Timing of Turbidite Sedimentation on the Mississippi Fan. Aapg Bulletin-American Association of Petroleum Geologists 77, 1129-1141.
Laberg, J.S., Vorren, T.O., 2000. The Traenadjupet Slide, offshore Norway - morphology, evacuation and triggering mechanisms. Marine Geology 171, 95-114.
Laberg, J.S., Vorren, T.O., Dowdeswell, J.A., Kenyon, N.H., Taylor, J., 2000. The Andoya Slide and the Andoya Canyon, north-eastern Norwegian-Greenland Sea. Marine Geology 162, 259-275.
Lastras, G., Canals, M., Urgeles, R., De Batist, M., Calafat, A.M., Casamor, J.L., 2004. Characterisation of the recent BIG'95 debris flow deposit on the Ebro margin, Western Mediterranean Sea, after a variety of seismic reflection data. Marine Geology 213, 235-255.
Lebreiro, S.M., McCave, I.N., Weaver, P.P.E., 1997. Late Quaternary turbidite emplacement on the Horseshoe abyssal plain (Iberian margin). Journal of Sedimentary Research 67, 856-870.
Lee, H.J., 2009. Timing of occurrence of large submarine landslides on the Atlantic Ocean margin. Marine Geology 264, 53-64.
Leynaud, D., Mienert, J., Vanneste, M., 2009. Submarine mass movements on glaciated and non-glaciated European continental margins: A review of triggering mechanisms and preconditions to failure. Marine and Petroleum Geology 26, 618-632.
Luttrell, K., Sandwell, D., 2010. Ocean loading effects on stress at near shore plate boundary fault systems. Journal of Geophysical Research-Solid Earth 115, B08411.
Manspeizer, W., Cousminer, H.L., 1988. Late Triassic-Early Jurassic synrift basins of the U.S. Atlantic margin. Geological Society of America, Boulder.
Maslin, M., Mikkelsen, N., Vilela, C., Haq, B., 1998. Sea-level- and gas-hydrate-controlled catastrophic sediment failures of the Amazon Fan. Geology 26, 1107-1110.
Maslin, M., Vilela, C., Mikkelsen, N., Grootes, P., 2005. Causes of catastrophic sediment failures of the Amazon Fan. Quaternary Science Reviews 24, 2180-2193.
Masson, D.G., Harbitz, C.B., Wynn, R.B., Pedersen, G., Lovholt, F., 2006. Submarine landslides: processes, triggers and hazard prediction. Philosophical Transactions of the Royal Society a-Mathematical Physical and Engineering Sciences 364, 2009-2039.

Paull, C.K., Buelow, W.J., Ussler, W., Borowski, W.S., 1996. Increased continental-margin slumping frequency during sea-level lowstands above gas hydrate-bearing sediments. Geology 24, 143-146.
Peltier, W.R., Fairbanks, R.G., 2006. Global glacial ice volume and Last Glacial Maximum duration from an extended Barbados sea level record. Quaternary Science Reviews 25, 3322-3337.
Piper, D.J.W., Cochonat, P., Morrison, M.L., 1999. The sequence of events around the epicentre of the 1929 Grand Banks earthquake: initiation of debris flows and turbidity current inferred from sidescan sonar. Sedimentology 46, 79-97.
Piper, D.J.W., Mosher, D.C., Gauley, B.J., Jenner, K., Campbell, D.C., Locat, J., Mienert, J., Boisvert, L., 2003. The Chronology and Recurrence of Submarine Mass Movements on the Continental Slope Off Southeastern Canada, Submarine Mass Movements and Their Consequences. Springer Netherlands, pp. 299-306.
Popenoe, P., Schmuck, E.A., Dillon, W.P., 1993. The Cape Fear landslide: Slope failure associated with salt diapirism and gas hydrate decomposition.
Rodriguez, N.M., Paull, C.K., 2000. Data Report: 14C dating of sediment of the uppermost cape fear slide plain: constraints on the timing of this massive submarine landslide.
Sheridan, R.E., Musser, D.L., Glover, L., Talwani, M., Ewing, J.I., Holbrook, W.S., Purdy, G.M., Hawman, R., Smithson, S., 1993. Deep Seismic-Reflection Data of Edge United-States Mid-Atlantic Continental-Margin Experiment - Implications for Appalachian Sutures and Mesozoic Rifting and Magmatic Underplating. Geology 21, 563-567.
Smith, B.R., Sandwell, D.T., 2006. A model of the earthquake cycle along the San Andreas Fault System for the past 1000 years. Journal of Geophysical Research-Solid Earth 111.
Steckler, M.S., Watts, A.B., Thorne, J.A., 1988. Subsidence and basin modeling at the U.S. Atlantic passive margin. Geological Society of America, Boulder, CO.
Trincardi, F., Cattaneo, A., Correggiari, A., Mongardi, S., Breda, A., Asioli, A., 2003. Submarine slides during relative sea level rise: two examples from the eastern Tyrrhenian Margin. Kluwer, Boston.
Van Weering, T.C.E., Nielsen, T.v., Kenyon, N.H., Akentieva, K., Kuijpers, A.H., 1998. Large submarine slides on the NE Faeroe continental margin. Geological Society, London, Special Publications 129, 5-17.
Watts, A.B., 2001. Isostasy and Flexure of the Lithosphere. Cambridge University Press, Cambridge, UK.
Watts, A.B., Rodger, M., Peirce, C., Greenroyd, C.J., Hobbs, R.W., 2009. Seismic structure, gravity anomalies, and flexure of the Amazon continental margin, NE Brazil. Journal of Geophysical Research-Solid Earth 114.

Wilson, C.K., Long, D., Bulat, J., 2004. The morphology, setting and processes of the Afen slide. Marine Geology 213, 149-167.
Winkelmann, D., Geissler, W., Schneider, J., Stein, R., 2008. Dynamics and timing of the Hinlopen/Yermak Megaslide north of Spitsbergen, Arctic Ocean. Marine Geology 250, 34-50.
Wyer, P., Watts, A.B., 2006. Gravity anomalies and segmentation at the East Coast, USA continental margin. Geophysical Journal International 166, 1015-1038.
Zaragosi, S., Auffret, G.A., Faugeres, J.C., Garlan, T., Pujol, C., Cortijo, E., 2000. Physiography and recent sediment distribution of the Celtic Deep-Sea Fan, Bay of Biscay. Marine Geology 169, 207-237.